Analyst

Interdisciplinary detection science

www.rsc.org/analyst

Volume 136 | Number 22 | 21 November 2011 | Pages 4605–4856

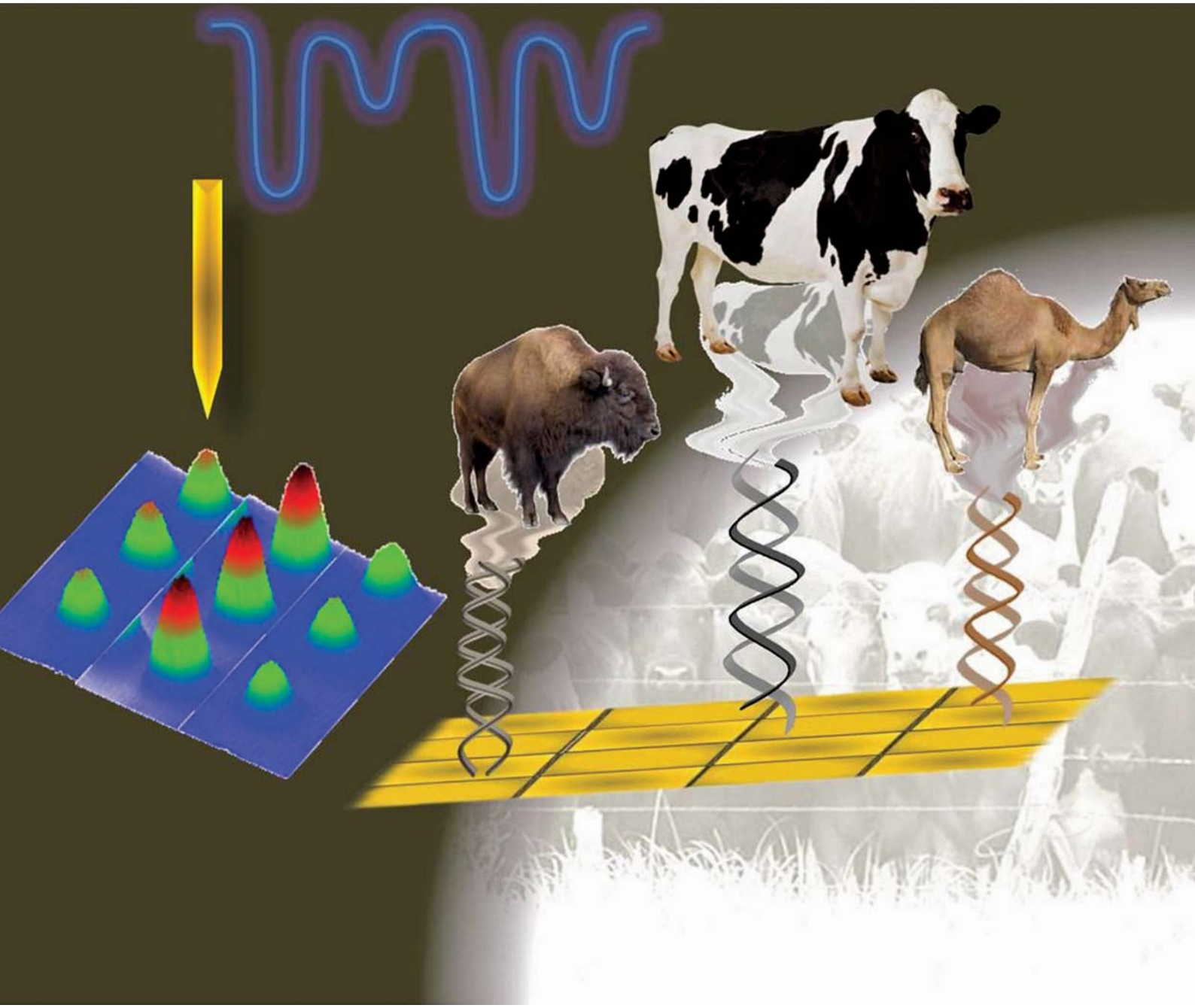

ISSN 0003-2654

RSC Publishing

HOT ARTICLE

Mohtashim Hassan Shamsi and Heinz-Bernhard Kraatz

Electrochemical identification of artificial oligonucleotides related to bovine species. Potential for identification of species based on mismatches in the mitochondrial cytochrome C_1 oxidase gene

Analyst

Dynamic Article Links

Cite this: *Analyst*, 2011, **136**, 4724

www.rsc.org/analyst

PAPER

Electrochemical identification of artificial oligonucleotides related to bovine species. Potential for identification of species based on mismatches in the mitochondrial cytochrome C_1 oxidase gene†‡

Mohtashim Hassan Shamsi[ab] and Heinz-Bernhard Kraatz*[ab]

Received 19th May 2011, Accepted 26th July 2011
DOI: 10.1039/c1an15414a

Our studies show that electrochemical impedance spectroscopy (EIS) and scanning electrochemical microscopy (SECM) of films of ds-DNA on gold allow us to distinguish between mitochondrial DNA fragments of the cytochrome c_1 oxidase (*mt-Cox*1) of three related species of the subfamily 'Bovinae' (*Bos taurus*, *Bison bison*, and *Bison bonasus*). In EIS, a perfectly matched DNA gives rise to a considerably larger charge transfer resistance R_{ct} compared to mismatched pairings. Differences in charge transfer resistance, ΔR_{ct}, before and after the addition of Zn^{2+} ions provide an additional tool for identification. In addition, all ds-DNA films were studied by SECM and their kinetic parameters were determined. Perfectly matched ds-DNAs are readily distinguished from mismatched duplexes by their lower rate constants. Our system can be used multiple times by dehybridization and rehybridization of capture strands up to the 250 pmole level.

Introduction

The emergence of a global food industry has made it necessary to find efficient and fail-proof methods to detect adulteration and/or admixtures in food products by manufacturers and suppliers. Reasons for this are based on cultural and religious restrictions and health and financial aspects.[1] Particularly meat is an important commodity in the global economy and the particular eating habits and preferences of different groups of people can polarize the market. For instance, the extensive demand of a particular species, such as cattle, in a market can create a huge gap between demand and supply, which ultimately entices the supplier to fulfil the demand by adding meat from cheaper species. Thus, it is critical to have efficient analytical tools to differentiate animal species even if they are closely related and belong to the same animal family or genus.

Recently, a range of PCR based methods were employed to identify animal species used in meat production. Such methods include real-time PCR,[2] nested primer PCR,[3] quantitative competitive (QC) PCR,[4] random amplification of polymorphic DNA (RAPD),[5] and PCR-based amplified fragment length polymorphism (AFLP).[6] The time required to carry out the amplications followed by testing restricts the use of such methods for in-field application and/or in portable detection systems.

Nucleic acids, DNA and RNA, are useful biomarkers, being part of all living organisms. The stability of DNA makes it a useful analytical target and it is no surprise that DNA targets were proposed as targets for the identification of species.[7] More recently, electrochemical techniques have been recognized as a fast, simple, sensitive, selective, miniaturizable and low cost tool to detect a DNA hybridization event.[8] The recent electrochemical methods employed to detect various food characteristics, such as tenderness, freshness, taste *etc.*, have been reviewed by E. Tamiya *et al.*[9] However, there have been very few attempts to detect and differentiate animal species electrochemically based on genomic DNA targets. For instance, Mascini *et al.* used inosine-modified (guanine free) captures to detect mammalian species belonging to different families through square wave voltametry.[10] Ahmed *et al.* employed an intercalating dye to detect different mammalian species by linear sweep voltammetry.[1] Our group has recently used scanning electrochemical microscopy (SECM) to analyze genomic DNA targets to differentiate animal species based on the occurrence of mismatches when DNA strands of two different animals were hybridized.[11]

While in principle useful, genomic DNA has a significant number of basepair variations between individuals, which render genomic targets useless for the identification of species. Recently, the 650-bp fragment of the 5′-end of the mitochondrial *Cox*1 gene has been considered a standard barcode sequence for

[a]*Department of Chemistry, University of Western Ontario, 1151 Richmond Street, London, Ontario, Canada N6A 5B7. E-mail: bernie.kraatz@utoronto.ca*
[b]*Department of Physical and Environmental Sciences, University of Toronto Scarborough, 1265 Military Trail, Toronto, Canada M1C 1A4*

† This article is part of a web theme in *Analyst* and *Analytical Methods* on Future Electroanalytical Developments, highlighting important developments and novel applications. Also in this theme is work presented at the Eirelec 2011 meeting, dedicated to Professor Malcolm Smyth on the occasion of his 60th birthday.

‡ Electronic supplementary information (ESI) available. See DOI: 10.1039/c1an15414a

animal identification, especially in the case of crustaceans and insects. It was also found effective in various animal groups, including vertebrates such as birds and fish.[12,13] Moreover, studies showed that most of the investigated species have distinct *Cox*1 barcode arrays with low variation within species and subspecies and high degrees of variance from closely linked taxa.[14] The recent report from Santamaria *et al.*[15] demonstrates that the *mt-Cox*1 gene distinguishes between different species, but does not possess significant intra-species variations as in the two *Bos* species *Bos taurus* and *Bos indicus*. What makes the use of *mt*-DNA targets even more useful is the fact that *mt*-DNA is available in multiple copies in a given cell (100–10 000 copies per cell), which facilitates its isolation, amplification and base-pair sequencing from small or even partly degraded samples.

Here we make use of synthetic 51-mer fragments of the mitochondrial *Cox*1 gene of the common cow (*Bos taurus*), the North American buffalo (*Bison bison*), and the European buffalo (*Bison bonasus*), all three belonging to the subfamily Bovinae.[16] We employ electrochemical impedance spectroscopy (EIS) and SECM to study the electrochemical response of films of double stranded *mt*-DNA prepared from capture and target strands of the three species. Moreover, in terms of practicability of our system, the surface immobilized ds-DNA were dehybridized and rehybridized with different complementary strands to check the variation between the prehybridized and surface hybridized response in EIS as well as in SECM. Hybridization of the 51-mer *Bos taurus* capture strand to *Bison bison* and *Bison bonasus* targets will result in 5 and 4 basepair mismatches, respectively. Hybridization of the 51-mer *Bison bison* capture strand to *Bos taurus* and *Bison bonasus* will give rise to 5 mismatches. Thus the problem of species identification is reduced to the problem of basepair mismatch identification. As we have shown before by EIS (and SECM), the presence of a mismatch in a ds-DNA film gives rise to significantly lower charge transfer resistances (higher charge transfer rates) in the presence of the anionic redox reporter $[Fe(CN)_6]^{3-/4-}$.[17] Thus, films prepared from hybridized capture and target strands should give rise to distinct EIS and SECM responses due to the presence of basepair mismatches within the films and should enable us to distinguish the three species from each other unequivocally based on basepair mismatches in mitochondrial DNA (*mt*-DNA) fragments.

Experimental

Reagents

Potassium ferrocyanide, potassium ferricyanide, trisodium EDTA, hydrogen peroxide (30%), sulfuric acid (98%) and perchloric acid (70%) were purchased from EM Science (Gibbstown, NJ) and used as received. Zinc(II) perchlorate hexahydrate and tris(hydroxymethyl)aminomethane (TRIS) were obtained from Aldrich (Milwaukee, WI) and Boehringer Mannheim Biochemicals (Indianapolis, IN), respectively. All solutions were prepared in deionized water (Millipore Milli-Q; 18 MΩ cm resistivity). The HPLC purified 51-mer oligonucleotide fragments of the mitochrondrial (mt) *Cox*1 gene modified at 5′-position with a 6-hydroxyhexyl disulfide and complementary sequences were synthesized at BioCorp (UWO OligoFactory, University of Western Ontario, London, ON). The oligonucleotides include 51-mer *mt-Cox*1 DNA of a *Bos taurus* (Holstein cow) capture strand **I** and a complementary strand **1**; a *Bison bison* (North American buffalo) capture strand **II** and a complementary strand **2**; and a *Bison bonasus* (European buffalo) complementary strand **3**. The oligonucleotide sequences of the capture strands (**I** and **II**) and complementary strands (**1–3**) are given in Table 1.

Preparation, polishing and regeneration of microelectrodes

The gold microelectrodes were prepared by sealing 50 μm diameter gold wires in glass capillaries in a way that one side was exposed as a flat surface for dsDNA film modification and the other side was joined to a copper extension for the outer connection. The gold surface was polished using a 3 micron polishing cloth followed by a 0.5 micron alumina surface. Further, electrochemical cleaning was performed by cyclic voltametry, 20 cycles each, first in 50 mM KOH and then in 0.5 M H_2SO_4 solutions in a potential range of −0.2 to +1.4 V *vs.* Ag/AgCl. The surface roughness was determined by integration of the gold oxide peak and is in the range of 1.5 to 2.0. The gold surfaces were regenerated after DNA chemisorption by applying potential pulses for 2 s at −1 V and +2 V, respectively, *vs.* Ag/AgCl in 50 mM KOH and 0.5 M H_2SO_4 followed by electrochemical cleaning as described above.

Preparation of double stranded DNA films

Double stranded DNA (dsDNA) were prepared by hybridizing an equimolar (50 μM) concentration of capture strand **I** or **II** and complementary strands **1**, **2** or **3** with a final strand concentration of 25 μM in a buffer solution of 50 mM Tris–ClO_4 (pH = 8.6). The prehybridized DNA films were formed on gold microelectrodes by incubating gold electrodes in 10 μL of 25 μM ds-DNA solution, containing 250 pmol ds-DNA molecules. The modified ds-DNA films were loaded with Zn^{2+} by incubating ds-DNA modified microelectrodes in 0.4 mM $Zn(ClO_4)_2 \cdot 6H_2O$ solution

Table 1 Sequence of the capture and complementary strands of *Bos taurus* (cow) and *Bison bison* (North American buffalo) and the complementary strand of *Bison bonasus* (European buffalo)

ss-DNA ID		Types of strands	Species
I	HO–$(CH_2)_6$–S–S–$(CH_2)_6$-5′-ACCTTCTTCGACCCGGCAGGAGGAGGAGACCCTATTCTATATCAACACTTA-3′	*Bos taurus*	Capture
II	HO–$(CH_2)_6$–S–S–$(CH_2)_6$-5′-ACCTTCTTCGACCCAGCAGGAGGAGGAGACCCCATCTTATACCAACACTTA-3′	*Bison bison*	
1	3′-TGGAAGAAGCTGGGCCGTCCTCCTCCTCTGGGATAAGATATAGTTGTGAAT-5′	*Bos taurus*	Complementary
2	3′-TGGAAGAAGCTGGGTCGTCCTCCTCCTCTGGGGTAGAATATGGTTGTGAAT-5′	*Bison bison*	
3	3′-TGAAAGAAGCTGGGCCGTCCTCCTCCTCTGGGGTAAGATATGGTTGTGGAT-5′	*Bison bonasus*	

in a buffer of 50 mM Tris–ClO_4 (pH 8.6) for 6 h at room temperature.

Dehybridization/rehybridization experiments

The prehybridized DNA films on gold surfaces were dehybridized by incubating the modified electrode or wafer in a 1 : 1 ethanol/DI water mixture for 15 min at the melting temperature of ~80 °C. Next, the dehybridized ss-DNA film was dried and rehybridized by incubating in a target strand solution (10 μL, 25 μM, pH 8.6) for 2 h at room temperature.

Electrochemical impedance measurements (EIS)

Electrochemical impedance measurements were performed on prehybridized, dehybridized and rehybridized DNA modified gold microelectrodes in a conventional three-electrode cell system. EIS measurements were also performed for prehybridized and rehybridized films in the presence of Zn^{2+}. The cell consisted of an Ag/AgCl reference electrode connected through a salt bridge, a Pt counter electrode and a DNA modified gold microelectrode as a working electrode. Impedance spectra were recorded using a CHI-650c system (CHI, Austin, TX) with the following parameters: AC voltage 5 mV amplitude, frequencies from 100 kHz to 0.1 Hz, at an applied potential of 250 mV *vs.* Ag/AgCl. All DNA modified electrodes were rinsed with buffer before each measurement. The measurements were made using at least ten different electrodes to obtain statistically meaningful results. All impedimetric results were fitted to a Randle's equivalent circuit, using ZSimpWin 2.0 software (Princeton Applied Research),[18] which allowed us to extract the resistive and capacitive components.

Scanning electrochemical microscopy

SECM measurements were made on a 200 nm thick gold substrate prepared by electron-beam deposition with a prior 20 nm thick Ti adhesion layer on a cleaned Si wafer having a 1 micron thick SiO_2 layer (Western's Nanofab). The gold substrate was cleaned in Piranha solution (70% sulfuric acid and 30% hydrogen peroxide) and thoroughly washed with DI water followed by drying under nitrogen before spotting the prehybridized ds-DNA. Spotting of the ds-DNA array onto flat gold substrates was achieved using a spotting robot (SpotBot, Telechem, Sunnyvale, CA). SECM experiments were performed with a CHI-900b (CH Instruments, Austin, TX). A Teflon cell was used with the 25 μm diameter Pt tip electrode (RG = 10), a Pt wire counter electrode, and an Ag/AgCl reference electrode. All measurements were performed in a 1 mM $K_4[Fe(CN)_6]$ solution made in a buffer mixture of 20 mM Tris–ClO_4 and 50 mM $NaClO_4$ (pH 8.6), proceeded by rinsing the surface with buffer. The tip potential was held constant at a formal potential, 500 mV, of $[Fe(CN)_6]^{4-}$ at a diffusion controlled rate. First, the bare gold was approached by the Pt tip through the use of a piezoelectric controlled motor. As the tip-to-substrate separation distance d decreases, a positive feedback is obtained due to an increase in the instantaneous tip current, I_T. The positive feedback confirms that the gold surface is clean and conductive. The approach was stopped when the tip current increased up to the level where current declines, *i.e.* ~11% of the tip current far away from the substrate $I_{T\infty}$ in a bulk solution. After initial positioning and approach, the tip was rastered over the substrate and the recorded tip current was normalized by I_T at the bare gold. Then, the DNA modified substrate was incubated in the Zn^{2+} solution as described above. After 6 h of incubation, the same procedure was repeated to scan ds-DNA in the presence of Zn^{2+}. The approach current was found to be higher by ~15% after Zn^{2+} addition. The SECM image was processed by software Gwyddion18 that converts the current response values into a colored image along with a color scale bar. The color scale appears with a random value which is normalized by the current infinity in order to get a normalized image and scale bar. Assuming irreversible substrate kinetics, a steady-state diffusion problem was solved for SECM geometry using the finite element method in COMSOL Multiphysics software.[19–21] Subsequently, theoretical approach curves were obtained which enabled us to extract kinetic information from the measurements.

Results and discussion

Impedimetric measurements

Electrochemical impedance spectroscopy (EIS) and scanning electrochemical microscopy (SECM) measurements were performed on thin films of hybridized ds-DNA attached through a 5′-disulfide linkage on gold surfaces. We focused on the use of two 5′-disulfide modified 51-mer *mt*-DNA fragments of the *Cox*1 gene of *Bos taurus* (common cow) **I** and *Bison bison* (North American buffalo) **II** acting as the capture strands for three unmodified 51-*mt*-DNA *Cox*1 fragments of *Bos taurus* (**1**), *Bison bison* (**2**) and European buffalo (*Bison bonasus*, **3**) complementary strands. All three species belong to the subfamily 'Bovinae'. The DNA sequence of the capture and complementary strands and hybridized ds-DNA sequences are given in Tables 1 and 2, respectively. During film formation, the disulfide link is broken in the presence of gold followed by the attachment of the capture DNA-hexanethiol anchoring group along with the resulting mercaptyl hexanol molecule to the surface through Au–S linkage. This easy protocol is expected to immobilize equal number of ds-DNA strands and MCH blocking molecules on the surface.

The EIS of the ds-DNA films on 50 μm diameter gold electrodes was examined at room temperature in the presence of $[Fe(CN)_6]^{3-/4-}$ at pH = 8.6. Then, measurements were repeated after exposure of the ds-DNA films to Zn^{2+}. The ability of the anionic redox probe $[Fe(CN)_6]^{3-/4-}$ to penetrate the ds-DNA is affected by the presence of basepair mismatches within the DNA film. Furthermore, the presence of Zn^{2+} within the film amplifies the differences in the impedance responses between a DNA film composed of mismatched and fully matched ds-DNAs.[17,22–24] The measurements are sufficiently sensitive to distinguish mismatch positions on the basis of their impedance differences.[25] Moreover, a previous study in our lab shows that the Zn^{2+} can be a choice for signal amplification among the other divalent and trivalent metal ions due to its reversibility and non-disruptiveness to basepair binding.[26]

Fig. 1 shows the results of EIS measurements in the form of Nyquist plots of a ss-DNA film and ds-DNA films formed by the capture strands of *Bos taurus* (**I**) and *Bison bison* (**II**) with

Table 2 Sequence of the fully matched and mismatched hybridized DNA duplexes of *Bos taurus* (cow), *Bison bison* (North American Buffalo) and *Bison bonasus* (European buffalo). Mismatched base pairs are shown in underlined italics in the capture strand and bold in the complementary strand

ds-DNA ID		Species	Match type
I-1	5′-ACC-TTC-TTC-GAC-CCG-GCA-GGA-GGA-GGA-GAC-CCT-ATT-CTA-TAT-CAA-CAC-TTA-3′ 3′-TGG-AAG-AAG-CTG-GGC-CGT-CCT-CCT-CCT-CTG-GGA-TAA-GAT-ATA-GTT-GTG-AAT-5′	Homo[a]	Matched
I-2	5′-ACC-TTC-TTC-GAC-CC*G*-GCA-GGA-GGA-GGA-GAC-CC*T*-AT*T*-*C*TA-TA*T*-CAA-CAC-TTA-3′ 3′-TGG-AAG-AAG-CTG-GG**T**-CGT-CCT-CCT-CCT-CTG-GG**G**-TA**G**-**A**AT-AT**G**-GTT-GTG-AAT-5′	Hetero[b]	Mismatched
I-3	5′-AC*C*-TTC-TTC-GAC-CCG-GCA-GGA-GGA-GGA-GAC-CC*T*-ATT-CTA-TA*T*-CAA-CAC-*T*TA-3′ 3′-TG**A**-AAG-AAG-CTG-GGC-CGT-CCT-CCT-CCT-CTG-GG**G**-TAA-GAT-AT**G**-GTT-GTG-**G**AT-5′	Hetero	Mismatched
II-1	5′-ACC-TTC-TTC-GAC-CC*A*-GCA-GGA-GGA-GGA-GAC-CC*C*-AT*C*-*T*TA-TA*C*-CAA-CAC-TTA-3′ 3′-TGG-AAG-AAG-CTG-GG**C**-CGT-CCT-CCT-CCT-CTG-GGA-TA**A**-**G**AT-AT**A**-GTT-GTG-AAT-5′	Hetero	Mismatched
II-2	5′-ACC-TTC-TTC-GAC-CCA-GCA-GGA-GGA-GGA-GAC-CCC-ATC-TTA-TAC-CAA-CAC-TTA-3′ 3′-TGG-AAG-AAG-CTG-GGT-CGT-CCT-CCT-CCT-CTG-GGG-TAG-AAT-ATG-GTT-GTG-AAT-5′	Homo	Matched
II-3	5′-AC*C*-TTC-TTC-GAC-CC*A*-GCA-GGA-GGA-GGA-GAC-CCC-AT*C*-*T*TA-TAC-CAA-CAC-*T*TA-3′ 3′-TG**A**-AAG-AAG-CTG-GG**C**-CGT-CCT-CCT-CCT-CTG-GGG-TA**A**-**G**AT-ATG-GTT-GTG-**G**AT-5′	Hetero	Mismatched

[a] Homo = ds-DNA made of capture and complementary strands of the same species. [b] Hetero = ds-DNA made of capture and complementary strands of different species.

complementary strands **1** to **3** in the presence and absence of Zn^{2+}. Only combinations **I-1** and **II-2** are fully matched sequences while all other combinations contain basepair mismatches. The EIS results were analyzed with the help of a modified Randle's circuit (inset of Fig. 1), being composed of the solution resistance (R_s), an element accounting for the charge transfer resistance (R_{ct}) and pinhole resistance (R_x), the capacitive component of the film (C_m) and a constant phase equivalent (CPE). The values of the circuit elements are summarized in Table S1 (see ESI‡). The solution resistance, R_s, accounts for the uncompensated resistance between the reference electrode and the working electrode, which remains constant before and after the addition of Zn^{2+}. The R_x is a small resistance due to the pinholes in the film structure, which has no significant and regular change after the addition of Zn^{2+}. The film capacitance (C_m) accounts for the capacitance of the DNA modified gold surface. The film capacitance is expected to increase due to the accumulation of charge after the addition of Zn^{2+}. However, there are no systematic variations of C_m. The constant phase equivalent (CPE) is considered as a non-ideal capacitor accounting for the inhomogeneity of the film and the electrode surface when n is close to 1.[27] The charge transfer resistance, R_{ct}, is the resistance related to the charge transfer between the redox probe and the electrode depending on the condition of the electrode surface. R_{ct} is strongly affected by the presence of basepair mismatches within the DNA sequence caused by changes in the ability of the anionic redox probe $[Fe(CN)_6]^{3-/4-}$ to diffuse into the ds-DNA film.[28] Films formed from fully matched DNA give rise to higher R_{ct}, while those containing basepair mismatches will have more structural defects within the film and thus pose less of a barrier for the redox probe to diffuse into. Thus, R_{ct} is a diagnostic factor that allows us to distinguish matched from mismatched DNA films. It is noteworthy to point out that the values for R_{ct} are double compared to those of earlier studies on 25-mer ds-DNA under similar conditions.[25] It is contrary to that observed from the studies based on ss-DNA and ds-DNA where the R_{ct} decreased with the length of the strand.[29,30] The reason for this disagreement may be different experimental conditions such as (a) equal number of ds-DNA and MCH immobilized and (b) the prehybridized ds-DNA used rather than surface hybridization in the present study (Scheme 1).

The addition of Zn^{2+} to the ds-DNA film reduces the repulsion of the negative redox probe and thus facilitates the charge transfer across the ds-DNA film which gives rise to changes in the charge transfer resistance R_{ct}. Differences in charge transfer resistance before and after Zn^{2+} addition (ΔR_{ct}) are larger for fully matched ds-DNA films. Smaller values of ΔR_{ct} indicate the presence of mismatches. In the case of the capture probes **I** and **II**, the combinations **I-1** and **II-2**, representing fully matched combinations of *Bos taurus* and *Bison bison*, show larger values for ΔR_{ct} compared to the mismatch combinations **I-2**, **I-3**, **II-1**, and **II-3** (see Table S1, ESI‡). The change in charge transfer resistance, ΔR_{ct}, as a function of a DNA duplex is shown in Fig. 2. Interestingly, the ΔR_{ct} of mismatched sequences (**I-2**, **I-3**, **II-1**, and **II-3**) is not well distinguishable which shows that addition of Zn^{2+} cannot discriminate the ds-DNA films possessing multiple mismatches.

The correlation between the ΔR_{ct} and the structure of the mismatched DNA duplexes is complex due to several variables, including the mismatch type, its position and the number of mismatches. Therefore, it is not easy to distinguish the various mismatched duplexes. However, it is interesting to note that the ds-DNA **I-2** and **II-1**, which are the two "hetero" duplexes of *Bos taurus* and *Bison bison*, have an equal number of mismatches at the same location but opposite in types (5′ *vs.* 3′). Their R_{ct} values before and after Zn^{2+} addition are approximately the same.

Scanning electrochemical microscopy

Next in our study, we examined the ds-DNA films by SECM. With the help of a spotting robot, an array of the prehybridized ds-DNA samples **I-1**, **I-2**, **I-3**, **II-1**, **II-2**, and **II-3** was spotted on a gold surface and incubated in a humid container to ensure the immobilization of the ds-DNA films on the surface through Au–S linkage. Then, the bare gold surface near the ds-DNA array was approached by a biased Pt-tip in the presence of a solution based redox probe, $[Fe(CN_6)]^{4-}$, and a positive feedback was obtained due to the redox cycling of $[Fe(CN_6)]^{4-}/[Fe(CN_6)]^{3-}$ between the tip and the conductive substrate. The degree of positive feedback depends on the conductive nature as well as the cleanliness of the substrate. Next, the ds-DNA array was scanned in the xy-plane at a constant tip–substrate distance and the

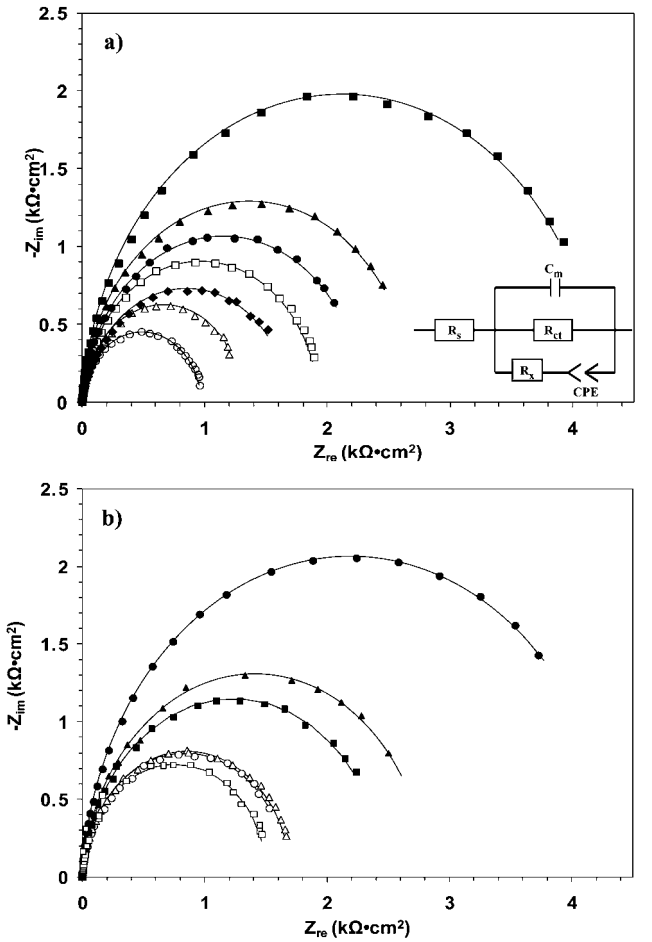

Fig. 1 (a) Representative Nyquist plots ($-Z_{im}$ *vs.* Z_{re}) for a ss-DNA (**1**) (◆); a fully matched dsDNA film (**I-1**) made of a *Bos taurus* probe (**I**) and its complementary strand (**1**) in the absence (■) and presence (□) of Zn^{2+}; a hybrid film (**I-2**) made of a *Bos taurus* probe (**I**) and a mismatched complementary strand of *Bison bison* (**2**) in the absence (▲) and presence (△) of Zn^{2+}; and a hybrid film (**I-3**) made of a *Bos taurus* probe (**I**) and a mismatched complementary strand of *Bison bonasus* (**3**) in the absence (●) and presence (○) of Zn^{2+}. (b) Representative Nyquist plots ($-Z_{im}$ *vs.* Z_{re}) for a fully matched dsDNA film (**II-2**) made of a *Bison bison* probe (**II**) and its complementary strand (**2**) in the absence (●) and presence (○) of Zn^{2+}; a hybrid film (**II-1**) made of a *Bison bison* probe (**II**) and a mismatched complementary strand of *Bos taurus* (**1**) in the absence (■) and presence (□) of Zn^{2+}; and a hybrid film (**II-3**) made of a *Bison bison* probe (**II**) and a mismatched complementary strand of *Bison bonasus* (**3**) in the absence (▲) and presence (△) of Zn^{2+}. Inset of (a) shows the corresponding modified Randle's equivalent circuit used in all cases. Black solid lines are fitting curves on the symbolized experimental curves by modified Randle's equivalent circuit.

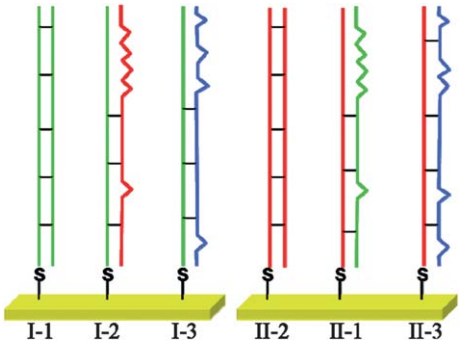

Scheme 1 Schematic shows the homo (matched) and hetero (mismatched) DNA duplexes immobilized on gold surfaces through Au–S linkage. Homo (**I-1**) *Bos taurus* probe and complementary strand, hetero (**I-2**) *Bos taurus* probe with *Bison bison* complementary, hetero (**I-3**) *Bos taurus* probe with *Bison bonasus* complementary, homo (**II-2**) *Bison bison* probe and complementary, hetero (**II-1**) *Bison bison* probe with *Bos taurus* complementary, and hetero (**III-3**) *Bison bison* probe with *Bison bonasus* complementary strands.

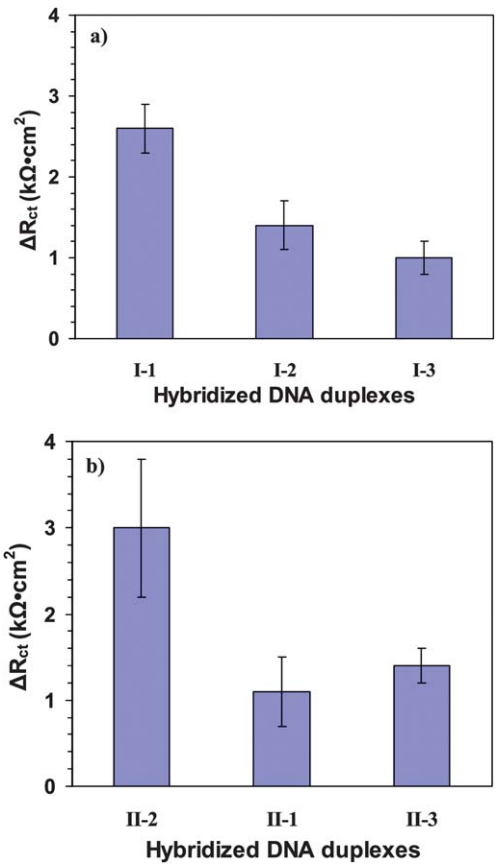

Fig. 2 Plots show a change in charge transfer (ΔR_{ct}), before and after addition of Zn^{2+}, (a) as a function of a homo-duplex of *Bos taurus* (**I-1**) and its hetero-duplexes with *Bison bison* (**I-2**) and *Bison bonasus* (**I-3**) and (b) as a function of a homo-duplex of *Bison bison* (**II-2**) and its hetero-duplex with *Bos taurus* (**II-1**) and *Bison bonasus* (**II-3**).

feedback current was recorded. The current response of the ds-DNA modified surface was transformed into a colored image as shown in Fig. 3. The current profile (current response at a specific distance between the tip and substrate) across the ds-DNA spots, shown by a black line in the color image, is given in Fig. S1 (ESI‡). The lower current response observed for all ds-DNA films, compared to the bare gold surface, is due to the hindrance in regeneration of $[Fe(CN)_6]^{4-}$ by blocking the conductive surface in the vicinity. The lowest current responses were observed for films of the perfectly matched duplexes **I-1** and **II-2**. Films containing mismatches (**I-2**, **I-3**, **II-1** and **II-3**) exhibit significantly higher feedback currents since they are more diffusive to the redox probe attributed to the low surface coverage

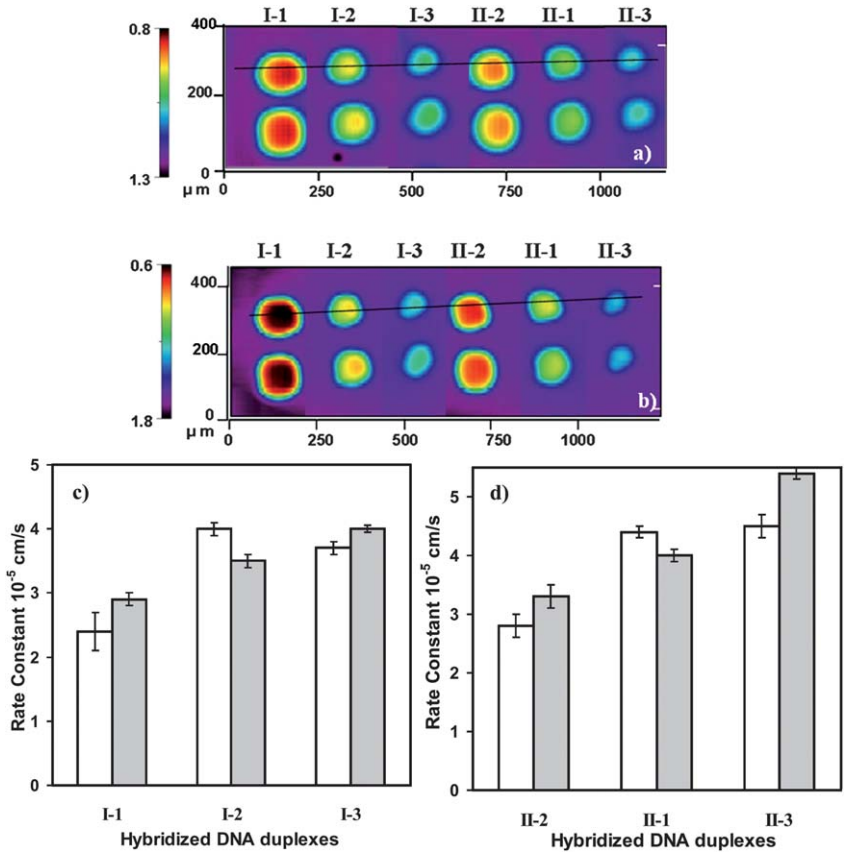

Fig. 3 Scanning electrochemical microscopic images of the homo (**I-1**) and (**II-2**) and hetero DNA duplexes (**I-2**), (**I-3**), (**II-1**) and (**II-3**) before (a) and after (b) the addition of Zn^{2+}. The color scale bar shows the intensity of current. The coordinates scale bar shows the area of the measured scan in micrometres. Black lines over spots represent the current profile extracted in Fig. S1(a) in the ESI.‡ Quantitative estimation of the rate of the reaction over the individual dsDNA spot is shown in (c) and (d). White and grey bars show rate constants before and after the addition of Zn^{2+}, respectively. The values of the rate constants (see ESI‡) were obtained through the theoretical modeling of the experimental approach curves over the individual dsDNA spot (see Fig. S1 (a) and (b) in the ESI‡).

compared to fully matched ds-DNA films as shown in Fig. 3 and the structural defects due to the presence of mismatches. The addition of Zn^{2+} amplified the current signal as shown in the current profile in Fig. S1, ESI.‡

For a quantitative evaluation of the current responses of the ds-DNA array, each DNA spot was individually approached at the centre from a vertical distance before and after addition of Zn^{2+}. Then, the approach curves (tip current *vs.* tip–surface distance) were generated as shown in Fig. S1 (see ESI‡). Kinetic parameters for the redox cycling of $[Fe(CN_6)]^{4-}/[Fe(CN_6)]^{3-}$ between the tip and the substrate were extracted from the approach curves by fitting into theoretical curves using the finite element method of irreversible kinetics. A theoretical model on experimental curves allows us to calculate the apparent rate constant, k^0, as described in Table S2 in the ESI.‡ Fig. 3(c) and (d) represent the plot between the apparent rate constants, k^0, *vs.* ds-DNA duplexes before and after addition of Zn^{2+}.

It is evident that both fully matched duplexes **I-1** and **II-2** exhibit the lowest rate constant, while all mismatched duplexes resulted in a larger k^0 making it easy to distinguish matched from mismatched duplexes. As for EIS measurements on these systems, the discrimination between the different mismatched duplexes remains a challenge. Addition of Zn^{2+} increases the rate constants of all duplexes, while the rate constants of mismatched duplexes of *Bos taurus* and *Bison bison* **I-2** and **II-1** were decreased after addition of Zn^{2+}. This interesting result may be an effect of the position of mismatch since both duplexes have same number of mismatched base pairs at same positions. This result can be useful in order to discriminate the hetero duplex **I-2** from **I-3** and **II-1** from **II-3**. Moreover, it is difficult to compare precisely the results obtained from EIS with the results from SECM due to the different technical approaches. However, the SECM results are in general agreement with the EIS results.

Dehybridization/rehybridization

In order to check the practicability of our system, we also performed dehybridization/rehybridization experiments on the ds-DNA modified gold surfaces for the *Bos taurus* system **I-1** and probed the system initially by EIS.

For this purpose, films of **I-1** were evaluated by EIS before and after dehybridization in a 1 : 1 ethanol and water mixture at the melting temperature, T_m, resulting in a R_{ct} of 1.25 kΩ·cm^2 as shown in Fig. 4. Next, the film was rehybridized with *Bison bison* (**2**) to form a mismatched duplex **I-2** (R_{ct} up to ~2.9 kΩ·cm^2). After incubation of this film in Zn^{2+}, the charge transfer

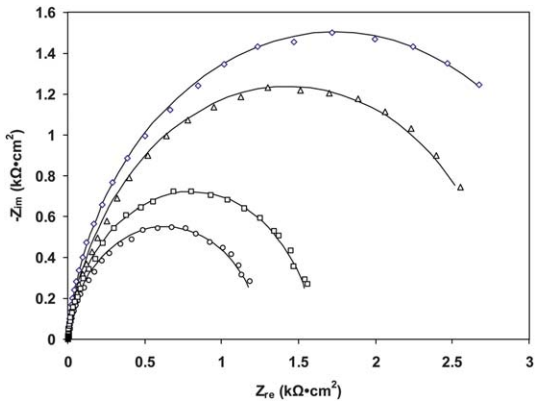

Fig. 4 Nyquist plots ($-Z_{im}$ *vs.* Z_{re}) for a prehybridized homo-duplex film of *Bos taurus* (**I-1**) in the absence of Zn^{2+} (◇), a dehybridized ssDNA film of a probe *Bos taurus* (**I**) in the absence of Zn^{2+} (○), a rehybridized hetero-duplex film of *Bos taurus* with *Bison bison* (**I-2**) in the absence (△) and presence (□) of Zn^{2+}. Black solid lines are fitting curves on the symbolized experimental curves using the modified Randle's equivalent circuit as given in Fig. 1(a).

resistance decreased to 1.6 kΩ·cm^2. The change in charge transfer resistance, ΔR_{ct}, ~1.3 kΩ·cm^2 is in close agreement with the prehybridized ΔR_{ct} value of the hetero duplex (**I-2**) of ~1.4 kΩ·cm^2.

Fig. 5 shows the results of a SECM study for the small array of **I-1** and **II-2** following the same dehybrdization/rehybridization protocol. The following steps were followed: (a) first gold surface was modified with an array of prehybridized homo duplexes **I-1** and **II-2**; (b) next, the array of **I-1** and **II-2** was dehybridized as described above removing the complementary strands and leaving capture strands **I** and **II** tethered to the surface; and (c) lastly, rehybridization with target strand **1** that resulted in perfectly matched **I-1** and mismatched **II-1** duplexes. The relative current responses of both arrays are similar before and after dehybridization; however, after rehybridization the duplex **I-1** showed considerably lower feedback current when compared with the mismatched duplex **II-1**.

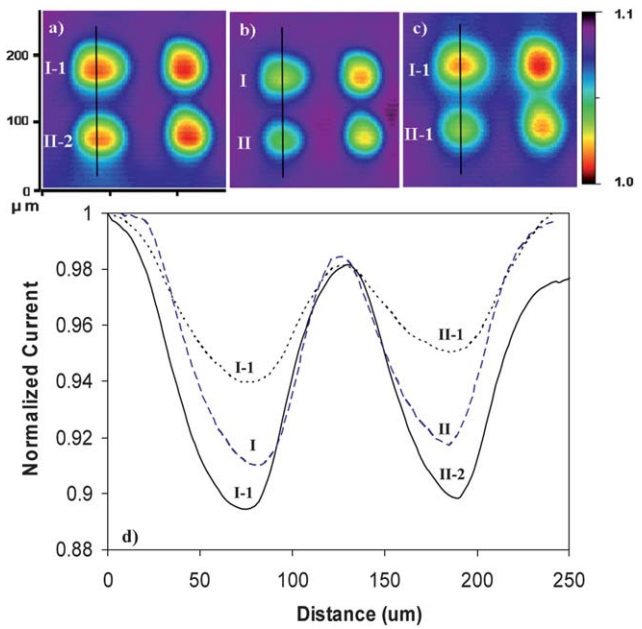

Fig. 5 SECM images of (a) prehybridized homo-duplex films of *Bos taurus* (**I-1**) and *Bison bison* (**II-2**), (b) dehybridized probe strands of *Bos taurus* (**I**) and *Bison bison* (**II**), and (c) rehybridized homo-duplex films of *Bos taurus* (**I-1**) and hetero-duplex films of *Bison bison* with *Bos taurus* (**II-1**). The color scale bar shows the intensity of current for which the current profile was extracted in (d). The coordinate scale shows the area of the scan in micrometres. (d) Current profile (normalized current *vs.* distance) of (a) prehybridized (solid line), (b) dehybridized (dashed line) and (c) rehybridized (dotted line) DNA films extracted from the SECM image above.

Conclusion

In the present work, we addressed here the question if it is possible to discriminate different species belonging to the same subfamily by simple electrochemical methods. Our study focused on the bovine species *Bos taurus* (cattle), *Bison bison* (North American buffalo) and *Bison bonasus* (European Buffalo) and exploited a 51-mer nucleotide fragment of their mitochondrial *Cox*1 gene. Combined EIS and SECM studies clearly show that (a) *mt*-DNA is a useful approach for species identification electrochemically, (b) SECM studies can be used to distinguish different DNA samples based on the presence of mismatches, and (c) the system is sufficiently robust to enable dehybridization/rehybridization of the DNA films without jeopardizing the ability for sequences identification. EIS and SECM give characteristic electrochemical responses for perfectly matched ds-DNA films and for films containing mismatches. A high ΔR_{ct} coupled with a low feedback current indicates the presence of perfectly matched DNA strands. While our work does not represent a sensing device, it clearly shows how our approach might be used in a putative device. For example, it can be envisioned that a sensor chip is fabricated aimed at the detection of contamination of processed meats. Such a sensor chip has to be composed of DNA fragments (*e.g. Cox*1 *mt*-DNA) of a series of known contaminants aimed at the detection of DNA fragments of the contaminant.

Acknowledgements

Financial support from NSERC in the form of a strategic grant is appreciated. Additional support from the University of Western Ontario, Department of Chemistry is appreciated. We also wish to thank Western's Nanofabrication facility for giving us access to the facility.

References

1 M. U. Ahmed, Q. Hasan, M. M. Hossain, M. Saito and E. Tamiya, *Food Control*, 2010, **21**, 599–605.
2 V. Fajardo, I. Gonzalez, I. Martin, M. Rojas, P. E. Hernandez and T. Garcia, *et al.*, *J.–Assoc. Off. Anal. Chem.*, 2008, **91**, 103–111.
3 A. P. Miguel and P.-V. Begona, *Food Chem.*, 2004, **86**, 143–150.
4 C. Wolf and J. Luthy, *Meat Sci.*, 2001, **57**, 161–168.
5 J. H. Calvo, P. Zaragoza and R. Osta, *Poult. Sci.*, 2001, **80**, 522–524.
6 S. Sasazaki, K. Itoh, S. Arimitsu, T. Imada, A. Takasuga and H. Nagaishi, *et al.*, *Meat Sci.*, 2004, **67**, 275–280.
7 F. Pereira, J. Carneiro and A. Amorim, *Recent Pat. DNA Gene Sequences*, 2008, **2**, 187–200.
8 T. G. Drummond, M. G. Hill and J. K. Barton, *Nat. Biotechnol.*, 2003, **21**, 1192–1199.

9 M. U. Ahmed, M. M. Hossain and E. Tamiya, *Electroanalysis*, 2008, **20**, 616–626.
10 M. Mascini, M. D. Carlo, M. Minunni, B. Chen and D. Compagnone, *Bioelectrochemistry*, 2005, **67**, 163–169.
11 P. M. Diakowski and H. B. Kraatz, *Chem. Commun.*, 2011, **47**, 1431–1433.
12 P. D. Hebert, A. Cywinska, S. L. Ball and J. R. deWaard, *Proc. R. Soc. London, Ser. B*, 2003, **270**, 313–321.
13 R. D. Ward, T. S. Zemlak, B. H. Innes, P. R. Last and P. D. N. Hebert, *Philos. Trans. R. Soc. London, Ser. B*, 2005, **360**, 1847–1857.
14 M. Hajibabaei, M. A. Smith, D. H. Janzen, J. J. Rodriguez, J. B. Whitfield and P. D. Hebert, *Mol. Ecol. Notes*, 2006, **6**, 959–964.
15 M. Santamaria, C. Lanave, S. Vicario and C. Saccone, *Biol. Chem.*, 2007, **388**, 943–946, The same study suggests that there is sufficient variation in the *mt*-ND1 gene that will allow barcoding of different cattle breeds.
16 Barcode of Life: http://www.boldsystems.org/views/taxbrowser.php?taxid=3121.
17 X. Li, Y. Zhou, T. C. Sutherland, B. Baker, J. S. Lee and H. B. Kraatz, *Anal. Chem.*, 2005, **77**, 5766–5769.
18 Princeton Applied Research electrochemical software: http://www.princetonappliedresearch.com/Our-Products/Electrochemical-Software/ZSimpWin.aspx.
19 C. Wei, A. J. Bard and M. V. Mirkin, *J. Phys. Chem.*, 1995, **99**, 16033–16042.
20 H. Xiong, J. Guo and S. Amemiya, *Anal. Chem.*, 2007, **79**, 2735–2744.
21 R. Zhu, Z. Qin, J. J. Noel, D. W. Shoesmith and Z. Ding, *Anal. Chem.*, 2008, **80**, 1437–1447.
22 X. Li, J. S. Lee and H. B. Kraatz, *Anal. Chem.*, 2006, **78**, 6096–6101.
23 Y. T. Long, C. Z. Li, H. B. Kraatz and J. S. Lee, *Biophys. J.*, 2003, **84**, 3218–3225.
24 Y. T. Long, C. Z. Li, T. C. Sutherland, H. B. Kraatz and J. S. Lee, *Anal. Chem.*, 2004, **76**, 4059–4065.
25 M. H. Shamsi and H. B. Kraatz, *Analyst*, 2010, **135**, 2280–2285.
26 X. Bin and H.-B. Kraatz, *Analyst*, 2009, **134**, 1309–1313.
27 M. Dijksma, B. A. Boukamp, B. Kamp and W. P. van Bennekom, *Langmuir*, 2002, **18**, 3105–3112.
28 M. Gebala, L. Stoica, S. Neugebauer and W. Schuhmann, *Electroanalysis*, 2009, **21**, 325–331.
29 A. B. Steel, R. L. Levicky, T. M. Herne and M. J. Tarlov, *Biophys. J.*, 2000, **79**, 975–981.
30 M. Revenga-Parra, T. García, F. Pariente, E. Lorenzo and C. Alonso, *Electroanalysis*, 2011, **23**, 100–107.